Available online at www.sciencedirect.com
SCIENCE DIRECT®
Physics of the Earth and Planetary Interiors 155 (2006) 249–259
PHYSICS OF THE EARTH AND PLANETARY INTERIORS
www.elsevier.com/locate/pepi

Elasticity of $CaSiO_3$ perovskite at high pressure and high temperature

Li Li [a,b,*], Donald J. Weidner [a,b], John Brodholt [a], Dario Alfè [a], G. David Price [a], Razvan Caracas [c], Renata Wentzcovitch [c]

[a] *Department of Earth Sciences, University College London, Gower Street, London WC1E6BT, UK*
[b] *Mineral Physics Institute, Department of Geosciences, University of New York at Stony Brook, Stony Brook, NY 11790, USA*
[c] *Department of Chemical Engineering and Material Science, Minnesota Supercomputing Institute, University of Minnesota, Minneapolis, MN 55455, USA*

Received 7 September 2005; received in revised form 2 December 2005; accepted 20 December 2005

Abstract

Ab initio molecular dynamic (AIMD) simulations were performed to calculate the equation of state (EOS) of $CaSiO_3$ perovskite at mantle pressure–temperature conditions. At temperatures above 2000 K, even though the hydrostatic crystal structure is metrically tetragonal in the pressure range of 13–123 GPa, the symmetry of the elastic moduli is consistent with cubic symmetry. Our results show that elastic constants and velocities are independent of temperature at constant volume. Referenced to room pressure and 2000 K, we find: Grűneisen parameter is $\gamma(V) = \gamma_0(V/V_0)^q$ with $\gamma_0 = 1.53$ and $q = 1.02(5)$, and the Anderson Grűneisen parameter is given by $(\alpha/\alpha_0) = (V/V_0)^{\delta_T}$ in which $\alpha_0 = 2.89 \times 10^{-5}\,K^{-1}$ and $\delta_T = 4.09(5)$. Using the third order Birch Murnaghan equation of state to fit our data, we have for ambient P and T, $K_0 = 236.6(8)$ GPa, $K_0' = 3.99(3)$, and $V_0 = 729.0(6)$ Å^3. Calculated acoustic velocities show the following P–T dependence: $(\partial \ln V_P/\partial V)_{T\,\mathrm{or}\,P} = -1.9 \times 10^{-3}$; $(\partial \ln V_S/\partial V)_{T\,\mathrm{or}\,P} = -1.5 \times 10^{-3}$; $(\partial \ln V_\Phi/\partial V)_{T\,\mathrm{or}\,P} = -2.4 \times 10^{-3}$; $(\partial \ln V_S/\partial \ln V_P)_{T\,\mathrm{or}\,P} = 0.79$; $(\partial \ln V_S/\partial \ln V_\Phi)_{T\,\mathrm{or}\,P} = 0.63$, indicating that the variations in bulk modulus overpower the variations in shear modulus.

The bulk modulus of $CaSiO_3$ perovskite is up to 10% lower than $MgSiO_3$ perovskite under lower mantle conditions. The difference diminishes with pressure and temperature. The shear modulus of $CaSiO_3$ perovskite is almost 25% lower compared with $MgSiO_3$ perovskite for shallow lower mantle pressures and temperatures and about 3% lower at the base of the lower mantle. The difference in density of these two perovskite is about 3–4% for all conditions. Both the density and bulk modulus differ from PREM by less than 2% throughout the lower mantle. The shear modulus is ∼10% lower at shallow depths grading to ∼5% by the core-mantle boundary. Thus, the seismic velocity of $CaSiO_3$ perovskite will be lower (0–6%) than PREM.

Keywords: $CaSiO_3$ perovskite; Lower mantle; Equations of state; Thermal expansion; Elastic constants; Grűneisen parameters; Thermoelastic properties

1. Introduction

$CaSiO_3$ perovskite is one of the most significant minerals in the earth (Funamori et al., 2000; Hirose et al., 1999; Liu and Ringwood, 1975; Mao et al., 1977; McDonough and Sun, 1995; Wood, 1997). Experimen-

* Corresponding author.
E-mail address: lilli@ic.sunysb.edu (L. Li).

0031-9201/$ – see front matter © 2006 Elsevier B.V. All rights reserved.
doi:10.1016/j.pepi.2005.12.006

tal investigations of the elastic properties of $CaSiO_3$ perovskite give various results: a cubic Pm3m structure with high bulk modulus ($K_0 \geq 275$ GPa) (Mao et al., 1989; Tamai and Yagi, 1989; Tarrida and Richet, 1989; Yagi et al., 1989), a cubic structure with significantly lower bulk modulus ($K_0 \sim 232$ GPa) (Shim and Duffy, 2000; Shim et al., 2000; Wang et al., 1996), a tetragonal structure with $K_0 = 255(5)$ GPa (Shim et al., 2002), and an even lower $K_0 = 212(7)$ GPa was predicted from perovskite analogues (Sinelnikov et al., 1998). Some studies (Hama and Suito, 1998; Shim et al., 2002; Wang et al., 1996; Wentzcovitch et al., 1995) suggested that $CaSiO_3$ perovskite can be regarded as invisible in modelling the lower mantle, while others (Sinelnikov et al., 1998) suggest that $CaSiO_3$ perovskite cannot be ignored due to an estimated shear modulus that is 37% lower than (Mg, Fe)SiO_3 perovskite. $CaSiO_3$ perovskite has stimulated a number of theoretical calculations (Akber-Knutson et al., 2002; Caracas and Wentzcovitch, 2005; Chizmeshya et al., 1996; Hemley et al., 1987; Jung and Oganov, 2005; Karki and Crain, 1998; Magyari-Kope et al., 2002a; Magyari-Kope et al., 2002b; Sherman, 1993; Stixrude et al., 1996; Warren et al., 1998; Wentzcovitch et al., 1995; Wolf and Bukowinski, 1987). The debate among the results from theoretical calculation is as contentious as those from experiments; see review in Jung and Oganov (2005).

In general, there are two critical issues: what are the stable structures and what are their elastic properties including both bulk and shear moduli. Since $CaSiO_3$ perovskite is not stable below 1 GPa and 1100 K (Gasparik et al., 1994; Swamy and Dubrovinsky, 1997) and is unquenchable, resolving the structure and elastic properties of $CaSiO_3$ perovskite demands high-resolution experimental tools (Shim and Duffy, 2000; Shim et al., 2002). The structural and energy differences between several structures are small (Akber-Knutson et al., 2002; Caracas and Wentzcovitch, 2005; Jung and Oganov, 2005) making theory difficult to assess the stable structure even at 0 K. In the past decade, the predictive power of the first-principle calculations has been continuingly growing. Using ab initio molecular dynamics (AIMD), elastic constants of materials can be calculated by monitoring the stress–strain relations (Oganov et al., 2001a; Oganov et al., 2001b; Stackhouse et al., 2004). Recent studies using density functional theory (DFT) have explored the stable structures for $CaSiO_3$ perovskite at 0 K. This paper extends these studies to provide single crystal elastic moduli to high temperature (5000 K) for the stable phases using density functional theory coupled with molecular dynamics.

2. Computational method

Ab initio molecular dynamics simulations were performed to calculate the elastic constants of $CaSiO_3$ perovskite using VASP code (Kresse and Furthmüller, 1996a; Kresse and Furthmüller, 1996b). The exchange-correlation functional E_{xc} used was the PW91 form of the generalized gradient approximation (GGA) (Perdew et al., 1992; Wang and Perdew, 1991). We used projector-augmented-wave (PAW) implementation of density functional theory and the implementation of an efficient extrapolation for the charge density (Alfè, 1999; Blöchl, 1994; Kresse and Joubert, 1999). All calculations were performed using an 80-atom super-cell. A plane-wave cut-off energy 500 eV was shown to be sufficient for the elastic constants to converge. Increasing the plane-wave cut-off to 1000 eV caused the calculated enthalpy difference of the two phases to change by less than 0.5 meV per atom and the absolute value of the elastic constants to differ by an average of 0.6%. The calculations were therefore considered converged. Γ point was used for sampling the Brillouin zone. The time step used in the dynamical simulation was 1 fs. The core radii used were 2.3 a.u. for Ca (core configuration $1s^2\ 2s^2\ 2p^6$), 1.9 a.u. for Si ($1s^2\ 2s^2\ 2p^6$) and 1.52 a.u. for O ($1s^2$). The equilibrium structure was obtained after at least 2ps of simulation (Fig. 1). Applying positive and negative strains (1 and 2%) to the equilibrated structure, stresses were calculated after 1ps simulation. Tests show that longer simulation has little effect on the calculated results. The kinetic pressure correction was used in our calculations. Error analysis for the stresses were performed following the algorithm described elsewhere (Allen and Tildesley, 1997).

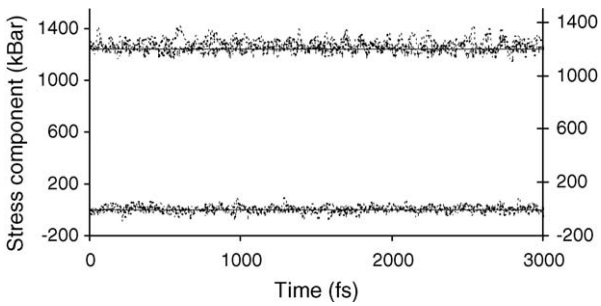

Fig. 1. Fluctuations of the stress components for the $CaSiO_3$ perovskite optimized at 124 GPa and 4000 K show that the stress is hydrostatic. Positive and negative strain (three axial strains for orthorhombic structure, two for tetragonal structure and one triclinic strain with magnitude of 1 and 2%) were applied on the hydrostatic structure, the time averages of the induced stresses were calculated. Isothermal elastic constants c_{ij} were derived from nonlinear stress–strain relations.

The acoustic velocities as a function of crystallographic direction were derived from the calculated single crystal elastic constants using the Christoffel equation (Nye, 1957). The measure of elastic anisotropy reported is the ratio of the fastest acoustic velocity to the slowest one.

3. Stable phase

The perovskite structure can have several subtle variations in atom positions that give rise to a variety of space groups at high P and T (Glazer, 1972; Glazer, 1975). The rotation and distortion of the octahedral units define these variations. Physical properties such as elastic moduli can radically change between phases and within the phase boundary region. Finite strain can be the agent of moving from one phase to another or to interchange twins within a single phase.

At 0 K, several variations of the perovskite structure compete for the minimum energy (Akber-Knutson et al., 2002; Caracas and Wentzcovitch, 2005; Jung and Oganov, 2005; Magyari-Kope et al., 2002a; Stixrude et al., 1996; Warren et al., 1998; Wentzcovitch et al., 1995) with the most recent conclusion being that the cubic phase is not stable at any pressure (P). Increasing temperature (T) should favour the higher symmetry phases, but the boundaries of these phase transitions need to be identified. In a companion paper (Li et al., 2005), we explore the stability fields of the high temperature $CaSiO_3$ perovskite through analysis of rotation angle of the octahedra, calculated X-ray diffraction patterns, and analysis of stresses on the fixed super-cell from quantum molecular dynamic calculations. Our conclusion is that there is a single stable phase between 1000 and 4000 K for the pressure range studied (15–130 GPa), as illustrated in Fig. 2. The cell dimensions of the hydrostatically stressed structures are listed in Table 1. Both orthorhombic and cubic symmetries of the perovskite phase are

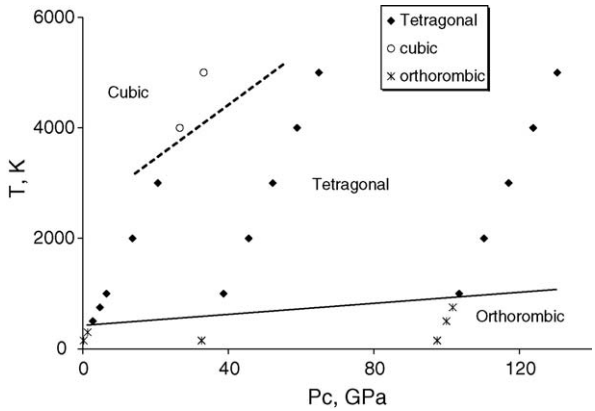

Fig. 2. Calculated phase diagram of $CaSiO_3$ perovskite. Below the solid line, orthorhombic phase is stable; above the dashed line, cubic phase is stable. The tetragonal phase that dominates the plot is tetragonal on an instantaneous time scale (1 fs).

Table 1
Cell parameters a, b and c, volume V, and stress tensor components σ_{11}, σ_{22} and σ_{33} at different P–T

T (K)	a (Å)	b (Å)	c (Å)	V (Å^3)	P_C (GPa)	σ_{11}	σ_{22}	σ_{33}
0	10.2521	10.2118	7.1694	750.59	−9.0	0	0	0
0	10.0038	10.0598	7.018	706.27	6.0	15	15	15
0	9.7439	9.6618	6.7724	637.48	41.0	50	50	50
0	9.4217	9.4217	6.5283	572.59	94.9	103.9	103.9	103.9
150	10.1117	10.1592	7.0913	728.46	−0.7	8.3(0)	8.3(1)	8.3(1)
1000	10.1216	10.1216	7.1112	728.52	5.7	14.7(1)	14.8(2)	14.7(2)
2000	10.1334	10.1334	7.0945	728.51	12.8	21.8(2)	21.7(2)	22.0(3)
3000	10.1169	10.1169	7.1179	728.53	19.8	28.8(3)	29.0(3)	28.6(3)
4000	10.1236	10.1236	7.1085	728.52	26.0	35.0(4)	35.0(4)	35.1(4)
150	9.7977	9.7195	6.8129	648.78	35.5	44.3(1)	44.5(1)	44.8(1)
1000	9.7810	9.7810	6.8510	655.37	37.7	46.6(3)	46.6(2)	46.9(3)
2000	9.7698	9.7698	6.8663	655.38	44.5	53.7(2)	53.3(2)	53.4(3)
3000	9.7624	9.7624	6.8768	655.39	51.1	60.4(3)	60.2(3)	59.6(4)
4000	9.7760	9.7760	6.8575	655.37	57.7	67.1(3)	66.0(3)	67.0(4)
150	9.4143	9.3121	6.5336	572.78	96.3	105.5(1)	105.2(0)	105.4(1)
1000	9.3451	9.3451	6.5592	572.82	102.5	111.4(4)	111.8(4)	111.3(3)
2000	9.3416	9.3416	6.5642	572.82	109.6	118.9(4)	118.4(3)	118.5(4)
3000	9.3420	9.3420	6.5635	572.82	116.6	125.7(3)	125.4(5)	125.8(5)
4000	9.3472	9.3472	6.5561	572.82	122.8	131.5(4)	132.1(3)	131.7(4)

V is the volume of a cell containing 80 atoms. The non-hydrostatic deviations of the stress tensor components are small (less than 0.5 GPa) from the average pressure. Errors for the stress tensor components are calculated using the same algorithm as described elsewhere (Alfe et al., 2000) and listed in the parenthesis.

present in a limited region. The "tetragonal" phase that dominates the diagram is tetragonal at any instant (1 fs time step), but the orientation of the tetragonal symmetry can vary with time (1 ps). The time average structure may be manifested as cubic. This is distinct from the "cubic" phase which is cubic at each time step. The tetragonal symmetry can be stabilized with a super-cell which has a unique axis parallel to the Si–O–Si bonds and the other two axes rotated 45° from the Si–O–Si bonds (i.e. the Pnma setting). Details are discussed in our companion paper (Li et al., 2005).

4. Ferroelastic strain relate to the c_{ij} calculation

The definition of a single crystal elastic constant is the ratio of the stress to an imposed infinitesimal strain. The nature of molecular dynamics calculation requires a large enough strain for the stress to be large enough to overcome the noise effect from the lattice vibrations. We use strains of 1 and 2% for such calculations. However, $CaSiO_3$ perovskite has ferroelastic spontaneous strains of less than 1% in the non-cubic phases. An example of the strain energy associated with strain coincident with the ferroelastic spontaneous strain is shown in Fig. 3. The two energy minima are at two macroscopic strains but represent two identical twins of the same structure. The forces are given by the derivative of the energy with respect to strain. Infinitesimal strain perturbations will encounter significant forces while finite strains may not properly sample the forces. Thus, in our calculations, we must take this effect into consideration. We used four criteria to confirm that the elastic moduli we calculated are indeed the infinitesimal elastic moduli: (1) check the linear stress–strain relation; (2) check the symmetry of the force in the positive and negative strain region; (3) check the symmetry of c_{ij} by redundant calculations; and (4) compare the bulk modulus calculated from c_{ij} and from volume perturbations. Table 2 gives the bulk modulus that is calculated from the single crystal elastic constants and directly from a volume strain. The agreement between the models is within the calculation errors, giving evidence that the results are not affected by ferroelastic transformations.

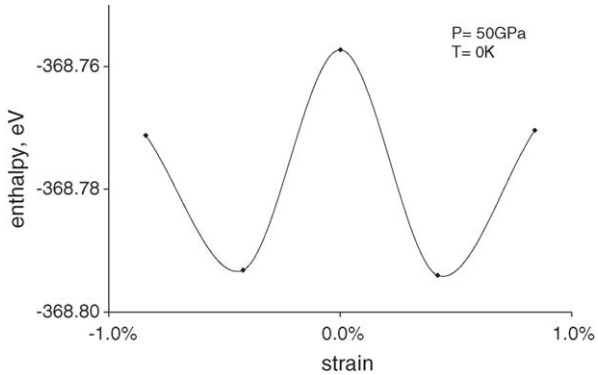

Fig. 3. Enthalpy vs. strain at 50 GPa and 0 K. Strain equals to $(a - b)/a$. Enthalpy is for the 80 atoms cell. The minima of enthalpy represent the equivalent twins of the same structure. The cubic phase corresponds to zero strain and is less stable (higher energy) than the distorted phases.

Table 2
Isothermal bulk modulus of $CaSiO_3$ perovskite

T (K)	P_C (GPa)	K_V (GPa)	K_R (GPa)	K_{RVH} (GPa)	$K(P, V)$ (GPa)
2000	12.8	226.0	226.0	226.0	228.6
3000	19.8	225.1	225.1	225.1	228.4
4000	26.0	235.8	235.8	235.8	224.3
2000	44.5	370.5	367.5	369.0	372.7
3000	51.1	372.0	371.8	371.9	374.3
4000	57.7	367.0	366.7	366.8	376.3
2000	109.6	620.9	620.9	620.9	599.5
3000	116.6	610.7	610.6	610.6	611.7
4000	122.8	607.1	606.4	606.8	609.0

Subscripts V, R and RVH represent Voigt, Reuss, Voigt–Reuss–Hill models. K_V, K_R and K_{RVH} are calculated from c_{ij}; $K(P, V)$ are the calculated pressure change induced by volume strain.

Table 3
Summary of thermoelastic parameters for $CaSiO_3$ perovskite compared with previous results

Parameter	Wang et al. (1996)	Shim et al. (2002)	This study
K_{T0}, GPa	232	236(4)	236.6(8)
K'_{T0}	4.8	3.9(2)	3.99(3)
α_0, 10^{-5}, K^{-1}	3.55(18)	2.2(3)	3.22(16)
$(\partial\alpha/\partial T)_P$, 10^{-9}	[0]	–	6.88(4.0)
$(\partial^2 P/\partial T^2)_V$, $GPa^2\,K^{-2}$	[0]	–	3.3(1.2)
$(\partial K/\partial T)_P$, $GPa\,K^{-1}$	−0.036(8)	−028(11)	−036(4)
V_0, $Å^3$	729.28	729.28	729.0(6)

[0] represent an assumed zero in the study.

5. *P–V–T* equation of state (EOS)

A goal of this study is to define the *P–V–T* equation of state of $CaSiO_3$ perovskite at mantle pressures and temperatures. There are two issues to be addressed: (1) the consistency between the calculated and the experimental data; and (2) within this context, the need for a pressure correction for the GGA calculations. Here we combine the *P–V–T* experimental data from Wang et al. (1996) with our calculated *K–V–T* to define one EOS. The EOS parameters of this calculation are listed in Table 3 along with that of Wang et al. (1996) for the *P–V–T* data alone. The experimental EOS is in good agreement with the combined experimental–theoretical EOS. The comparison underscores the compatibility of the theoretical models with the experimental observations and bolsters our confidence to use the theoretical inferences in the *P–T* range of the mantle, outside of the region studied experimentally.

An overestimate of pressure due to the GGA approximation has been generally observed (Li et al., 2005; Oganov et al., 2001b; Wentzcovitch et al., 1995). In our previous study (Li et al., 2005), we resolved this issue by correcting the pressure for an Al and Fe bearing $MgSiO_3$ perovskite by fitting the bulk modulus–volume (*K–V*) results to a Birch–Murnaghan (B–M) relation but with a V_0 fixed by experimental data. The B–M relation was then used to calculate pressure from the *V* of the model calculation. We found that the GGA pressure overestimated the B–M pressure consistently by 8 GPa, a value which varies little with pressure. This result suggests that the GGA-based calculation is precise in defining state properties as a function of *V*, but that it overestimates, by a constant value the pressure for any volume. In the current study, this procedure needs to be modified since $CaSiO_3$ perovskite is unquenchable to room pressure and V_0 has not been measured in a reliable fashion (Wang et al., 1996). Instead, we use an internally consistent set of experimental *P–V–T* data as discussed above to define the EOS illustrated in Table 3 which in turn is used to calculate *P* for all of the theoretical *V–T* points. We find that the pressure defined by the GGA-based calculation is 9 ± 1 GPa higher than the EOS pressure. This value appears to be relatively independent of either pressure or temperature and agrees well with the correction that we concluded for $MgSiO_3$ perovskite. We correct the GGA pressure by this amount throughout the text and refer to the corrected pressure as P_C.

The calculations for state variables that are performed here are for temperatures of 2000 K or higher. Since the ultimate goal is to project these properties into the Earth's lower mantle and not to room temperature/pressure, we define a new reference condition at 2000 K and room pressure. Above, we have established good agreement with the low pressure—low temperature data and obtained a pressure correction for the GGA-based calculations. To calculate the reference state variables we use the K_T versus P_C and the *V* versus P_C calculations at 2000 K and fit a third order Birch–Murnaghan equation of state solving for $K_0(2000\,K) = 171(4)$ GPa, $K_0'(2000K) = 4.75(7)$, and $V_0(2000\,K) = 778(2)$ Å^3. We will use these values as the reference state in the following sections.

6. Thermal expansion, α

With the theoretical models in good agreement with low pressure data in defining the room pressure–temperature equation of state parameters, we now turn to define equation of state properties in the pressure and temperature range of the lower mantle. The calculations yield elastic moduli and pressure at three temperatures for each of three volumes. No lattice instability indicating melting occurs even at 29 GPa and 4000 K as the material retains a large and positive shear modulus. Pressure versus temperature for three constant volumes is illustrated in Fig. 4. The slope of the curve $(\partial P/\partial T)_V$ is equal to αK_T where K_T is the isothermal bulk modulus. Thermal expansion α is thus obtained by $(\partial P/\partial T)_V/K_T$. As discussed below, the elastic moduli c_{ij}, and hence the bulk modulus K_T, are independent of temperature at constant volume within the uncertainty of these calculations in the *P*, *T* region explored. Since $(\partial P/\partial T)_V$ also appears constant at each volume, the thermal expansion becomes temperature independent at constant volume in the *P*, *T* space of these calculations. Thermal expansion at 2000 K as a function of pressure is listed in Table 4.

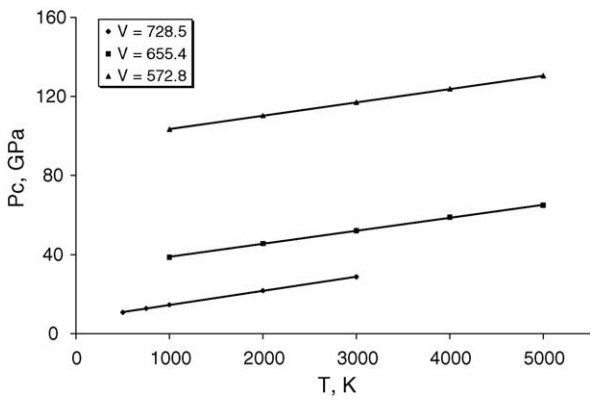

Fig. 4. Isochoric pressure vs. temperature for $CaSiO_3$ perovskite. P_C is the calculated pressure after GGA correction. Data plotted here are for the tetragonal structure only.

Table 4
Thermal expansion α and Grűneisen parameter γ at pressure and temperature

T (K)	P_C (GPa)	V (Å^3)	α ($\times 10^{-5}$ K^{-1})	$(\partial P/\partial T)_V$	γ
2000	12.8	728.52	2.96	0.0679	1.52
3000	19.8	728.51	2.96		1.53
4000	26	728.53	2.96		1.49
2000	44.5	655.37	1.78	0.0667	1.33
3000	51.1	655.38	1.78		1.33
4000	57.7	655.39	1.78		1.33
2000	109.6	572.82	1.1	0.0675	1.18
3000	116.6	572.82	1.1		1.18
4000	122.8	572.82	1.1		1.18

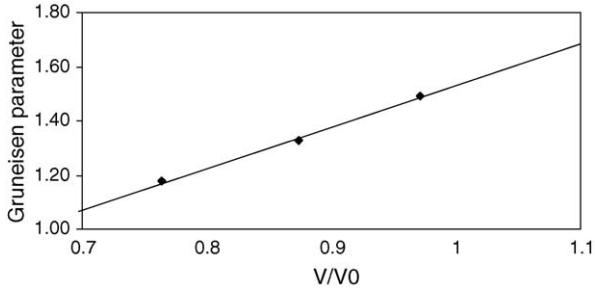

Fig. 5. $\gamma(V/V_0)$ function. Solid diamonds are the AIMD results. Solid line is the best fit with $\gamma = \gamma_0(V/V_0)^q$, where $\gamma_0 = 1.53$, $q = 1.0$, $V_0 = 729.0$ Å^3.

7. Grűneisen parameter, $\gamma(V)$

The Grűneisen parameter, $\gamma(V)$, is calculated from the thermal pressure and thermal energy: $\gamma(V) = P_{th}(V, T)V/E_{th}(V, T)$, where the thermal energy $E_{th} = 3(N-1)k_bT$, with the Boltzmann constant $k_b = 1.3807 \times 10^{-23}$ J/K, N is the number of atoms in the supercell, $N = 80$ in this study; details of the method are described in (Oganov et al., 2000; Oganov et al., 2001a). At $T \geq 2000$ K, γ varies little with T. The 0 K intercept of the isochors P_0 in Fig. 4 are used to in defining the $P_{th} = P(T) - P_0$. The calculated γ are listed in Table 4. The dependence of γ with volume is illustrated in Fig. 5. Fitting the relation: $\gamma = \gamma_0(V/V_0)^q$, we obtain $q = 1.02 \pm 0.05$.

8. Anderson Grűneisen parameter, δ_T

The Anderson Grűneisen parameter, δ_T, is given by $\delta_T = (\partial \ln \alpha/\partial \ln V)_T$. Fig. 6 illustrates α as a function of V and as a function of pressure at 2000 K, with a curve based on the best fit value of δ_T of 4.09 ± 0.05. Since the thermal expansion is, within the uncertainty, independent of temperature at constant volume, this value of δ_T is independent of temperature. The adiabatic Anderson Grűneisen, $\delta_T = \delta_S + \gamma$ can be obtained from $\delta_T = \delta_S + \gamma_0(V/V_0)^q$.

9. Single crystal elastic constants

A $2\sqrt{2} \times 2\sqrt{2} \times 2$ 80-atom cell with Pbnm atom positions (Oganov et al., 2001a), was used as the starting structure with the axes length appropriate for a metrically cubic system ($a = b = \sqrt{2}c$). At each pressure and temperature, we calculate the stresses. The dimensions of the box are then varied to produce a hydrostatic stress field. The differences in stresses are also manifest in the differences in the cell parameters in the hydrostatic conditions ($\sigma_{11} = \sigma_{22} = \sigma_{33}$; $\sigma_{ij} = 0$ when $i \neq j$). The elastic constants are then determined by applying a strain to the sample box and solving for the stress field. Strains of ± 2 and $\pm 1\%$ are used with the elastic modulus given by $c_{ij} = (\partial \sigma_i/\partial \varepsilon_j)$. The nine elastic constants for 150 K orthorhombic case are given in Table 5.

The elastic constants for the tetragonal phase are presented in Table 6 in the coordinate system of the cubic (aristotype) setting. Even though the hydrostatic crystal

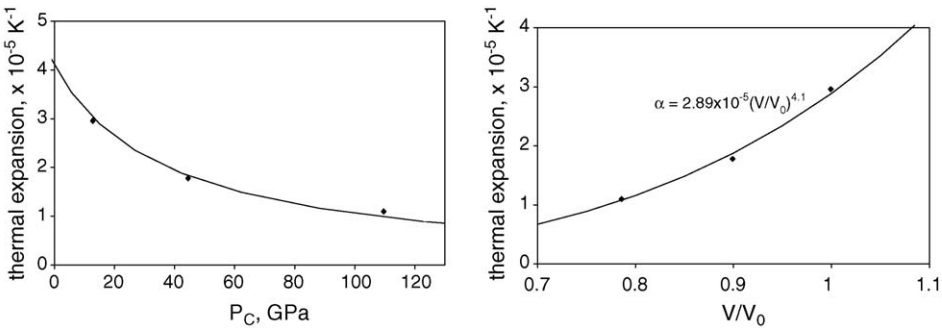

Fig. 6. The thermal expansion vs. pressure and volume. The pressure is projected onto a 2000 K isotherm. Within the computational uncertainty, the thermal expansion depends on pressure and temperature only through volume. The fitted line on both figures represents $\alpha_0 = 2.89 \times 10^{-5}$ K^{-1} and $\delta_T = 4.1$ with $V_0 = 729.0$ Å^3.

Table 5
Elastic moduli c_{ij} at pressure and temperature

T (K)	V (Å^3)	P_C (GPa)	c_{11} (GPa)	c_{22} (GPa)	c_{33} (GPa)	c_{12} (GPa)	c_{13} (GPa)	c_{32} (GPa)	c_{44} (GPa)	c_{55} (GPa)	c_{66} (GPa)
150	728.46	8.3	481	484	380	77	165	189	195	191	61
150	648.78	44.5	635	703	623	205	294	251	234	241	104
150	572.78	105.3	964	1060	941	395	468	371	286	314	128

The presented c_{ij} is in orthorhombic setting. The errors for the elastic constants are within 5%.

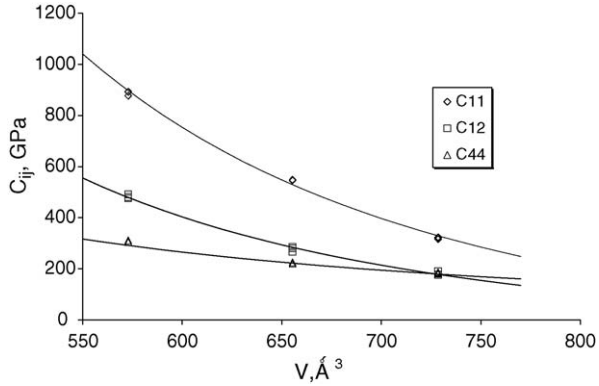

Fig. 7. Single crystal elastic moduli *cij* vs. volume for $CaSiO_3$ perovskite. Data plotted here are for 2000, 3000 and 4000 K and listed in Table 6. The dependences of c_{ij} on temperature at constant volume are negligible and are not distinguished in the plot.

structure is metrically tetragonal, the symmetry of the elastic moduli is consistent with cubic within the calculation errors. In addition, the dynamics of the tetragonal system is such that the structure may well be cubic on a time scale of a few pico seconds (see the companion paper (Li et al., 2005)). We, thus, restrict further discussion to the 'cubic' elastic moduli taken as the best fit cubic model of the tetragonal elastic moduli.

Fig. 7 illustrates the cubic elastic moduli as a function of volume for all temperatures. At constant volume, the elastic moduli are essentially constant, while they have significant volume dependence. We fit the single crystal elastic constants with a third order Eulerian strain equation of state (Bina and Helffrich, 1992) given by

$$c_{ij} = c_{ij}^0(1+2f)^{5/2}\left\{1-f\left[5-3\left(\frac{\partial c_{ij}^0}{\partial P}\right)\left(\frac{K_0}{c_{ij}^0}\right)\right]\right\} \quad (1)$$

where $f = 1/2[(V_0/V)^{2/3} - 1]$. The fitted finite strain values are compared with the calculated values in Fig. 7. The values of the c_{ij}^0 and their pressure derivatives are given in Table 7 where the reference state is 2000 K and room pressure.

10. Velocities

Acoustic velocities are calculated from the elastic moduli. With single crystal properties we are able to define acoustic anisotropy as well as the isotropic aggregate average. Table 8 gives the average acoustic velocities based on the Reuss–Voight–Hill adiabatic bulk properties along with the ratio of the maximum to minimum velocities and the maximum polarization velocity ratio for $CaSiO_3$ perovskite at the different P, T conditions.

Table 6
Elastic constants at P–T

T (K)	V (Å^3)	P_C (GPa)	c_{11} (GPa)	c_{33} (GPa)	c_{12} (GPa)	c_{13} (GPa)	c_{44} (GPa)	c_{66} (GPa)
2000	728.52	12.8	328	320	176	178	190	183
3000	728.51	19.8	326	317	177	174	180	183
4000	728.53	26.0	321	311	189	194	180	188
2000	655.37	44.5	508	583	255	278	237	202
3000	655.38	51.1	551	544	299	273	230	220
4000	655.39	57.7	547	550	301	260	219	220
2000	572.82	109.6	874	911	501	482	296	315
3000	572.82	116.6	866	888	486	475	301	322
4000	572.82	122.8	856	930	478	473	297	314

The presented c_{ij} are in cubic setting. The conversion from orthorhombic setting (Table 5) to cubic setting is done by $c_{11} = (c_{11} + c_{12} + 2c_{66})/2$; $c_{12} = (c_{11} + c_{12} - 2c_{66})/2$; $c_{66} = (c_{11} - c_{12})/2$, the rest of c_{ij} are unchanged.

Table 7
Isothermal thermoelastic properties at the reference condition of $T = 2000$ K and $P = 0$ GPa

	c_{11} (GPa)	c_{12} (GPa)	c_{44} (GPa)	K_{0T} (GPa)	μ_0 (GPa)	V_0 (Å^3)	ρ (g/cm^3)	γ_0	q	α_0 ($\times 10^{-5}$ K^{-1})	δ_T
X (2000 K)	234.7	128.0	157.1	170.9[a]	104.7	778.4[a]	3.965	1.63	1.0	3.78	4.1
$\partial X/\partial P$ (2000 K)	7.5	4.0	2.0	4.76[a]	1.9						

[a] EOS parameters calculated from K and V vs. P at 2000 K.

Fig. 8 illustrates the longitudinal, bulk, and shear velocities as a function of volume. The results for 2000, 3000, and 4000 K are all included in this figure with the observation that the velocity is independent of temperature at constant volume. We calculate the logarithmic derivative of velocity with respect to volume with the result that: $(\partial \ln V_P/\partial V)_{T \text{ or } P} = -1.9 \times 10^{-3}$; $(\partial \ln V_S/\partial V)_{T \text{ or } P} = -1.5 \times 10^{-3}$; $(\partial \ln V_\Phi/\partial V)_{T \text{ or } P} = -2.4 \times 10^{-3}$; $(\partial \ln V_S/\partial \ln V_P)_{T \text{ or } P} = 0.79$; $(\partial \ln V_S/\partial \ln V_\Phi)_{T \text{ or } P} = 0.63$ indicating that the variations in bulk modulus overpower the variations in shear modulus.

11. Geophysical implications

$CaSiO_3$ perovskite is third largest component of the lower with most Earth models suggesting an abundance of less than 10%vol. The contrast in properties between $CaSiO_3$ perovskite and $MgSiO_3$ perovskite (~80%vol. allow us to examine the role of $CaSiO_3$ perovskite in constraining lower mantle properties. Listed in Table 9 are the parameters for these two perovskites obtained from this study and from Oganov et al. (2001b) which also used AIMD methods. The listed data for FiO_3 perovskite

Table 8
Sound velocity V_P, V_S for $CaSiO_3$ perovskite at pressure and temperature

T (K)	P_C (GPa)	K_S (GPa)	μ (GPa)	V_P (km s^{-1})	V_S (km s^{-1})	ρ (g cm^{-3})	A_P	A_S	A_{SH}/A_{SV}
2000	12.8	249.2	129.5	9.98	5.53	4.24	1.22	1.61	1.59
3000	19.8	259.4	126.0	10.04	5.45	4.24	1.21	1.59	1.58
4000	26	263.9	117.9	9.97	5.28	4.24	1.24	1.78	1.76
2000	44.5	390.3	190.5	11.7	6.36	4.71	1.16	1.33	1.28
3000	51.1	400.9	182.8	11.7	6.23	4.71	1.11	1.35	1.35
4000	57.7	411.9	180.6	11.77	6.19	4.71	1.1	1.34	1.34
2000	109.6	615.1	255.3	13.31	6.88	5.39	1.09	1.28	1.28
3000	116.6	635.5	256.7	13.47	6.9	5.39	1.08	1.3	1.25
4000	122.8	640.6	258.5	13.52	6.93	5.39	1.09	1.29	1.25
150	-0.7	245.2	135.6	10.03	5.66	4.24	1.23	1.82	1.78
150	35.5	384.5	186.6	11.54	6.26	4.76	1.14	1.53	1.53
150	96.3	603.4	246.2	13.15	6.76	5.39	1.13	1.6	1.57

Adiabatic bulk and shear moduli are K_S and μ. A_P and A_S are the ratios between the fastest and lowest velocities for longitudinal and shear wave. $A_{SH/SV}$ is largest ratio of SH and SV velocities.

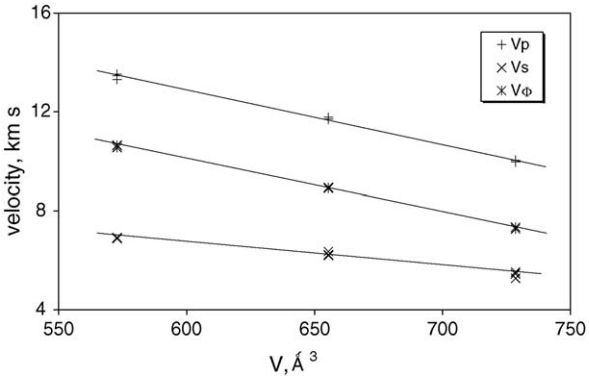

Fig. 8. Longitudinal, shear wave and bulk sound velocities vs. volume. Data presented here include 2000, 3000 and 4000 K. Data are listed in Table 7. The fitted solid lines give following results: $(\partial \ln V_P/\partial V)_{T \text{ or } P} = -1.9 \times 10^{-3}$; $(\partial \ln V_S/\partial V)_{T \text{ or } P} = -1.5 \times 10^{-3}$; $(\partial \ln V_\Phi/\partial V)_{T \text{ or } P} = -2.4 \times 10^{-3}$; $(\partial \ln V_S/\partial \ln V_P)_{T \text{ or } P} = 0.79$; $(\partial \ln V_S/\partial \ln V_\Phi)_{T \text{ or } P} = 0.63$.

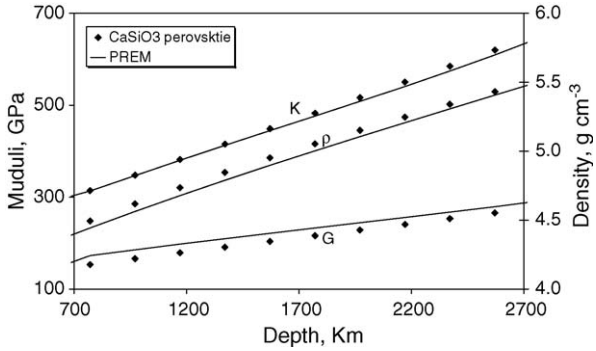

Fig. 9. Bulk, shear modulus and density of $CaSiO_3$ perovskite compared with PREM. Geotherm was taken from Brown and Shankland (1981).

are interpolated to the P and T conditions of Oganov et al. (2001b) using the EOS defined in Table 7 and Eq. (1). The table shows that the bulk modulus of $CaSiO_3$ perovskite can be as much as 10% lower than that of its Mg counterpart. The difference diminishes with pressure and temperature, although remaining above 7% at 3500 K and 88 GPa. The shear modulus of $CaSiO_3$ perovskite is almost 25% lower compared with $MgSiO_3$ perovskite at 38 GPa and 1500 K. The difference also decreases with pressure and temperature down to about 3% at 88 GPa and 3500 K. The difference in density of these two perovskite is about 3–4% for all conditions.

Based on the density and bulk modulus profiles, Wang et al. (1996) termed $CaSiO_3$ perovskite invisible. Their extrapolated bulk modulus and density were close to those of the Earth (PREM) implying that major changes in the amount of $CaSiO_3$ perovskite does not alter the mineral properties from PREM. Sinelnikov et al. (1998) have suggested that shear modulus of $CaSiO_3$ perovskite can be quite distinct from PREM based on low pressure studies on analogues. Our calculations allow us to investigate this issue at mantle conditions as illustrated in Fig. 9 where we show the bulk modulus, shear modulus and density projected along a geotherm (Brown and Shankland, 1981) compared with PREM. Both the density and bulk modulus agree well with the projection described by Wang et al. (1996) and differ from PREM by less than 2% throughout the lower mantle. The shear modulus, while close to PREM, is ∼10% lower at shallow depths grading to ∼5% by the core–mantle boundary. Thus, the seismic velocity of $CaSiO_3$ perovskite will be lower (0–6%) than PREM.

While $CaSiO_3$ perovskite appears to have a small affect on the seismic velocities, there remains the possibility that it can be significant in defining the Q of

Table 9
Comparison between the $MgSiO_3$ perovskite and $CaSiO_3$ perovskite

Parameters	$CaSiO_3$ perovskite					$MgSiO_3$ perovskite[a]				
P^a (GPa)	38	38	38	88	88	38	38	38	88	88
T^a (K)	1500	2500	3500	1500	3500	1500	2500	3500	1500	3500
P(2000 K) (GPa)	41.37	34.63	27.89	91.37	77.90					
V (Å^3)	660.89	674.194	689.022	590.78	606.121	147.63	150.83	154.08	132.55	136.48
K_T (GPa)	344.57	318.48	291.74	524.09	477.67	382.70	349.90	332.70	565.70	508.60
G (GPa)	171.65	161.83	151.69	237.82	220.91	214.30	194.90	166.20	269.70	226.90
ρ (g cm^{-3})	4.67	4.58	4.48	5.22	5.09	4.52	4.42	4.33	5.03	4.89
γ	1.38	1.41	1.44	1.24	1.27	1.30	1.37	1.40	1.21	1.26
α ($\times 10^{-5}$ K^{-1})	1.94	2.10	2.30	1.22	1.36	1.91	2.15	2.26	1.34	1.51
K_S (GPa)	358.41	342.08	325.55	535.99	506.50	396.80	375.80	369.50	579.40	542.50
V_P (km s^{-1})	11.21	11.04	10.86	12.78	12.54	12.29	11.99	11.69	13.66	13.15
V_S (km s^{-1})	6.06	5.95	5.82	6.75	6.59	6.89	6.64	6.20	7.32	6.81

$P(2000\text{ K}) = P^* - P(\text{thermal})$, $P(\text{thermal}) = T(\partial P/\partial T)_V$.
[a] Are the conditions from (Oganov et al., 2001b).

the lower mantle. Our calculations indicate that this material may be stable in a tetragonal structure involving a small spontaneous strain. Such phases normally exist with domains of different orientations separated by domain-wall boundaries. The domain walls move in response to stress and can be the source of acoustic absorption (Harrison et al., 2003), the greater absorption occurring close to the phase boundary. This could cause strong absorption of acoustic waves in the lower mantle. The clarification of this issue awaits further experimental exploration.

Acknowledgements

This work is support by NERC (Grant Nos. NER/T/S/2001/00855; NER/O/S/2001/01227), and computer facilities provided by NERC at University College London, and the High Performance Computing Facilities of the University of Manchester (CSAR) and the Daresbury Laboratory (HPCx). DJW acknowledges the Leverhulme Trust for support through the visiting Professor program. DJW and LL acknowledge NSF EAR-9909266, EAR0135551, EAR0135550, MPI 361. R. Wentzcovitch acknowledge NSF EAR-0135533 and ITR-0428774 (VLab).

References

Akber-Knutson, S., Bukowinski, M.S.T., Matas, J., 2002. On the structure and compressibility of $CaSiO_3$ perovskite. Geophys. Res. Lett. 29 (3), 1034.

Alfè, D., 1999. Ab-initio molecular dynamics, a simple algorithm for charge extrapolation. Comput. Phys. Commun. 118, 31–33.

Alfe, D., Kresse, G., Gillan, M., 2000. Structure and dynamics of iron under Earth's core conditions. Phys. Rev. B 61, 132.

Allen, M.P., Tildesley, D.J., 1997. Computer Simulation of Liquids, 408. Oxford University Press, New York, NY, USA.

Bina, C.R., Helffrich, G.R., 1992. Calculation of elastic properties from thermodynamic equation of state principles. Annu. Rev. Earth Planet Sci. 20, 527–552.

Blöchl, P.E., 1994. Projector augmented-wave method. Phys. Rev. B 50, 17953–17979.

Brown, J.M., Shankland, T.J., 1981. Thermodynamic parameters in the Earth as determined from seismic profiles. Geophys. J. R. Astr. Soc. 66, 579–596.

Caracas, R., Wentzcovitch, R.M., 2005. Equation of state and stability of $CaSiO_3$ under pressure. Geophys. Res. Lett. 32 (4), L06303.

Chizmeshya, A.V.G., Wolf, G.H., McMillan, P.F., 1996. First-principles calculation of the equation-of-state, stability, and polar optic modes of CaSiO (sub 3) perovskite. Geophys. Res. Lett. 23 (20), 2725–2728.

Funamori, N., Jeanloz, R., Miyajima, M., Fujuno, K., 2000. Mineral assemblages of basalt in the lower mantle. J. Geophys. Res., B Solid Earth Planets 105, 26037–26043.

Gasparik, T., Wolf, K., Smith, C.M., 1994. Experimental determination of phase relations in the $CaSiO_3$ system from 8 to 15 GPa. Am. Mineralogist 79 (11–12), 1219–1222.

Glazer, A.M., 1972. The classification of tilted octahedra in perovskites. Acta Cryst. B28, 3384.

Glazer, A.M., 1975. Simple ways of determining perovskite structures. Acta Cryst. A31, 756.

Hama, J., Suito, K., 1998. High-temperature equation of state of $CaSiO_3$ perovskite and its implications for the lower mantle. Phys. Earth Planetary Interiors 105, 33–46.

Harrison, R.J., Redfern, S.A.T., Street, J., 2003. The effect of transformation twins on the seismic-frequency mechanical properties of polycrystalline $Ca_{1-x}Sr_xTiO_3$ perovskite. Am. Mineralogist 88, 574–582.

Hemley, R.J., Jackson, M.D., Gordon, R.G., 1987. Theoretical study of the structure, lattice dynamics, and equation of state of perovskite-type $MgSiO_3$ and $CaSiO_3$. Phys. Chem. Miner. 14, 2–12.

Hirose, K., Fei, Y., Ma, Y.Z., Mao, H.K., 1999. The fate of subducted basaltic crust in the Earth's lower mantle. Nature (London) 397 (53–56).

Jung, D.Y., Oganov, A.R., 2005. Ab initio study of the high-pressure behavior of $CaSiO_3$ perovskite. Phys. Chem. Miner. 32 (N2), 146–153.

Karki, B.B., Crain, J., 1998. First-principles determination of elastic properties of $CaSiO_3$ perovskite at lower mantel pressures. Geophys. Res. Lett. 25 (14), 2741–2744.

Kresse, G., Furthmüller, J., 1996a. Efficiency of ab-initio total energy calculations for metals and semiconductors using a plane-wave basis set. Comput. Mater. Sci. 6, 15–50.

Kresse, G., Furthmüller, J., 1996b. Efficient iterative schemes for ab initio total-energy calculations using a plane-wave basis set. Phys. Rev. B 54, 11169.

Kresse, G., Joubert, D., 1999. From ultrasoft pseudopotentials to the projector augmented-wave method. Phys. Rev. B 59, 1758–1775.

Li, L., et al., 2005. Electronic spin state of ferric iron in Al-bearing perovskite in the lower mantle. Geophys. Res. Lett., submitted for publication.

Liu, L., Ringwood, A.E., 1975. Synthesis of a perovskite-type polymorph of $CaSiO_3$. Earth Planetary Sci. Lett. 14, 209–211.

Magyari-Kope, B., Vitos, L., Grimavall, G., Johansson, B., Kollar, J., 2002a. Low-temperature crystal structure of $CaSiO_3$ perovskite: an ab initio total energy study. Phys. Rev. B 65, 193107.

Magyari-Kope, B., Vitos, L., Grimavall, G., Johansson, B., Kollar, J., 2002b. Model structure of perovskite: cubic-orthorhombic phase transition. Comput. Mater. Sci. 25, 615–621.

Mao, H.K., Chen, L.C., Hemley, R.J., Jephcoat, A.P., Wu, Y., 1989. Stability and equation of state of $CaSiO_3$-perovskite to 134 GPa. J. Geophys. Res., B Solid Earth Planets 94, 17889–17894.

Mao, H.K., Yagi, T., Bell, P.M., 1977. Mineralogy of the earth's deep mantle: quenching experiments on mineral compositions at high pressure and temperature, Carnegie Institution of Washington Year Book, 1977, pp. 502–504.

McDonough, W.F., Sun, S.S., 1995. The composition of the Earth. Chem. Geol. 120, 223–253.

Nye, J.F., 1957. Physical Properties of Crystals. Oxford University Press, Ely House, London.

Oganov, A.R., Brodholt, J.P., Price, G.D., 2000. Comparative study of quasiharmonic lattice dynamics, molecular dynamics and Debye model applied to MgSiO (sub 3) perovskite. Phys. Earth Planetary Interiors 122 (3–4), 277–288.

Oganov, A.R., Brodholt, J.P., Price, G.D., 2001a. Ab initio elasticity and thermal equation of state of $MgSiO_3$ perovskite. Earth Planetary Sci. Lett. 184 (3–4), 555–560.

Oganov, A.R., Brodholt, J.P., Price, G.D., 2001b. The elastic constants of $MgSiO_3$ perovskite at pressures and temperatures of the Earth's mantle. Nature (London) 411 (6840), 934–937.

Perdew, J.P., et al., 1992. Atoms, molecules, solids, and surfaces: applications of the generalized gradient approximation for exchange and correlation. Phys. Rev. B 46, 6671–6687.

Sherman, D.M., 1993. Equation of state, elastic properties, and stabilities of $CaSiO_3$ perovskite—first-principles (periodic Hartree-Fock) results. J. Geophys. Res., B Solid Earth Planets 98, 19795–19805.

Shim, S.-H., Duffy, T.S., 2000. The stability and *P–V–T* equation of state of $CaSiO_3$ perovskite in the Earth's lower mantle. J. Geophys. Res., B Solid Earth Planets 105 (B11), 25955–25968.

Shim, S.-H., Duffy, T.S., Shen, G., 2000. The equation of state of $CaSiO_3$ perovskite to 108 GPa at 300K. Phys. Earth Planetary Interiors 120, 327–338.

Shim, S.-H., Jeanloz, R., Duffy, T.S., 2002. Tetragonal structure of $CaSiO_3$ perovskite above 20 GPa. Geophys. Res. Lett. 29 (24), 2166.

Sinelnikov, Y.D., Chen, G., Liebermann, R.C., 1998. Elasticity of $CaTiO_3$–$CaSiO_3$ perovskites. Phys. Chem. Miner. 25, 515–521.

Stackhouse, S., Brodholt, J.P., Wookey, J., Kendall, J.-M., Price, G.D., 2004. The effect of temperature on the seismic anisotropy of the perovskite and post-perovskite polymorphs of $MgSiO_3$. Earth Planetary Sci. Lett. 230 (1–2), 1–10.

Stixrude, L., Cohen, R.E., Yu, R., Krakauer, H., 1996. Prediction of phase transition in $CaSiO_3$ perovskite and implications for lower mantle structure. Am. Mineralogist 81, 1293–1296.

Swamy, V., Dubrovinsky, L.S., 1997. Thermodynamic data for the phase in the $CaSiO_3$ system. Geochim. Cosmochim. Acta 61, 1181–1191.

Tamai, H., Yagi, T., 1989. High-pressure and high-temperature phase relations in $CaSiO_3$ and $CaMgSi_2O_6$ and elasticity of perovsktie-type $CaSiO_3$. Phys. Earth Planetary Interiors 54, 370–377.

Tarrida, M., Richet, P., 1989. Equation of state of $CaSiO_3$ perovskite to 96 GPa. Geophys. Phys. Res. 16 (11), 1351–1354.

Wang, Y., Perdew, J.P., 1991. Correlation hole of the spin-polarized electron-gas, with exact small-wave-vector and high density scaling. Phys. Rev. B 44, 13298–13307.

Wang, Y., Weidner, D.J., Guyot, F., 1996. Thermal equation of state of $CaSiO_3$ perovskite. J. Geophys. Res., B Solid Earth Planets 101 (1), 661–672.

Warren, M.C., Ackland, G.J., Karki, B.B., Clark, S.J., 1998. Phase transitions in silicate perovskites from first principles. Mineralogical Mag. 62, 585–598.

Wentzcovitch, R.M., Ross, N.L., Price, G.D., 1995. Ab initio study of $MgSiO_3$ and $CaSiO_3$ perovskites at lower-mantle pressures. Phys. Earth Planetary Interiors 90 (1–2), 101–112.

Wolf, G.H., Bukowinski, M.S.T., 1987. Theoretical study of the structural properties and equation of state of $MgSiO_3$ and $CaSiO_3$ perovskite: implications for lower mantle composition. In: Syono, Y. (Ed.), High pressure Research in Mineral Physics. Terra Scientific, Tokyo.

Wood, B.J., 1997. Phase transformations and partitioning relations in peridotite under lower mantle conditions. Earth Planetary Sci. Lett. 174, 341–354.

Yagi, T., Kusanagi, S., Tsuchida, Y., Fukai, Y., 1989. Isothermal compression and stability of perovskite-type $CaSiO_3$. In: Proceedings of the Japan Academy of Science, pp. 129–132.